AGU PUBLICATIONS

Global Biogeochemical Cycles

RESEARCH ARTICLE

10.1002/2014GB005054

Key Points:
- Time scale of the silicate weathering feedback is reassessed to be ~240 kyr
- Ten percent of added carbon dioxide persists in the atmosphere on ~240 kyr time scale
- Twenty-one percent of peak global temperature anomaly persists on ~240 kyr time scale

Supporting Information:
- Text S1, Figure S1 and S2, and Tables S1 and S2

Correspondence to:
T. M. Lenton,
t.m.lenton@exeter.ac.uk

Citation:
Colbourn, G., A. Ridgwell, and T. M. Lenton (2015), The time scale of the silicate weathering negative feedback on atmospheric CO_2, *Global Biogeochem. Cycles*, *29*, 583–596, doi:10.1002/2014GB005054.

Received 2 DEC 2014
Accepted 1 APR 2015
Accepted article online 7 APR 2015
Published online 15 MAY 2015

The time scale of the silicate weathering negative feedback on atmospheric CO_2

G. Colbourn[1,2,3], A. Ridgwell[2], and T. M. Lenton[1]

[1]College of Life and Environmental Sciences, University of Exeter, Exeter, UK, [2]School of Geographical Sciences, University of Bristol, Bristol, UK, [3]School of Environmental Sciences, University of East Anglia, Norwich, UK

Abstract The ultimate fate of CO_2 added to the ocean-atmosphere system is chemical reaction with silicate minerals and burial as marine carbonates. The time scale of this silicate weathering negative feedback on atmospheric pCO_2 will determine the duration of perturbations to the carbon cycle, be they geological release events or the current anthropogenic perturbation. However, there has been little previous work on quantifying the time scale of the silicate weathering feedback, with the primary estimate of 300–400 kyr being traceable to an early box model study by Sundquist (1991). Here we employ a representation of terrestrial rock weathering in conjunction with the "GENIE" (Grid ENabled Integrated Earth system) model to elucidate the different time scales of atmospheric CO_2 regulation while including the main climate feedbacks on CO_2 uptake by the ocean. In this coupled model, the main dependencies of weathering—runoff, temperature, and biological productivity—were driven from an energy-moisture balance atmosphere model and parameterized plant productivity. Long-term projections (1 Myr) were conducted for idealized scenarios of 1000 and 5000 PgC fossil fuel emissions and their sensitivity to different model parameters was tested. By fitting model output to a series of exponentials we determined the *e*-folding time scale for atmospheric CO_2 drawdown by silicate weathering to be ~240 kyr (range 170–380 kyr), significantly less than existing quantifications. Although the time scales for reequilibration of global surface temperature and surface ocean pH are similar to that for CO_2, a much greater proportion of the peak temperature anomaly persists on this longest time scale; ~21% compared to ~10% for CO_2.

1. Introduction

The legacy of human perturbation of the global carbon cycle will be a long one [*Archer*, 2005; *Archer et al.*, 2009]. The burning of fossil fuels, deforestation, and to a lesser extent cement production, creates an excess of CO_2 in the atmosphere (and associated climatic changes) that will persist until it is sequestered either by natural and/or anthropogenic means. Leaving aside potential deliberate anthropogenic intervention in the form of geoengineering [*Royal Society*, 2009], we focus here on improving understanding of the long-term natural carbon sinks—primarily the order $10^3 - 10^5$ year geologic processes.

On short time scales ($\sim 10^0 - 10^1$ years), excess CO_2 is absorbed from the atmosphere by the terrestrial biosphere through the "CO_2 fertilization" effect, as well as forest regrowth. The input of carbon is partly transferred to the soil where it is broken down and returned back to the atmosphere as CO_2 (or CH_4) on a $\sim 10^1 - 10^2$ year time scale. At the same time, the ocean removes excess atmospheric CO_2, initially by CO_2 dissolving in and reacting with surface waters. Dissolved CO_2 forms carbonic acid, which quickly dissociates into bicarbonate and carbonate ions, allowing more CO_2 to enter the ocean from the atmosphere. This buffering allows approximately a factor of 10 more carbon to be absorbed by the ocean than would be the case were it to remain undifferentiated like oxygen [*Revelle and Suess*, 1957]. Both the land and ocean carbon sinks are thought to currently absorb ~30% each of the excess atmospheric CO_2, with the land sink being more variable on a multiyear time scale [*Le Quéré et al.*, 2009]. However, as more CO_2 enters the atmosphere, the immediate terrestrial and oceanic sinks become less able to absorb excess atmospheric CO_2 [*Canadell et al.*, 2007; *Le Quéré et al.*, 2007]. Indeed the airborne fraction of CO_2 (remaining over emitted, per annum) may have increased from 40% to 45% in recent decades [*Le Quéré et al.*, 2009].

The addition of CO_2 to seawater causes ocean acidification through the release of protons during the dissociation of carbonic acid into bicarbonate and the depletion of carbonate ions. Once the ocean is mixed down to depth, the reduced carbonate ion concentration causes the Carbonate Compensation Depth (CCD;

the depth in the ocean at which the rain flux of calcium carbonate, $CaCO_3$, is balanced by the dissolution rate of $CaCO_3$ in the sediments) to move upward, resulting in the dissolution of $CaCO_3$ sediments (equation (1)) on parts of the ocean floor now lying below the CCD.

$$CO_{2(aq)} + H_2O_{(l)} + CaCO_{3(s)} \longrightarrow Ca^{2+}_{(aq)} + 2HCO^{-}_{3(aq)} \quad (1)$$

Further sequestration of atmospheric CO_2 occurs through the weathering of terrestrial (calcium or magnesium) carbonate rocks; chemically, this involves the same reactions as those occurring between dissolved CO_2 in the ocean and sedimentary $CaCO_3$. Carbon dioxide dissolves in rain water to form a weak carbonic acid that accelerates the chemical weathering of the rocks, producing calcium and bicarbonate ions (equation (1); here given for calcium, but could equally be for magnesium) that are transported by rivers and ground water to the ocean. This process is known as "terrestrial neutralization" [*Archer et al.*, 1998; *Ridgwell and Hargreaves*, 2007].

Depending on the magnitude of the carbon emissions, the fraction of initial emissions remaining in the atmosphere after these processes have run to completion, is in the range 6–11% [*Goodwin and Ridgwell*, 2010; *Archer*, 2005]). The remaining fraction of anthropogenic carbon is removed from the atmosphere by the process of silicate weathering, whereby two moles of carbon are consumed for every one that is available for subsequent transfer back to the atmosphere from the ocean-sediment system (equation (2); compare with equation (1)):

$$2CO_{2(aq)} + H_2O_{(l)} + CaSiO_{3(s)} \longrightarrow Ca^{2+}_{(aq)} + 2HCO^{-}_{3(aq)} + SiO_{2(aq)} \quad (2)$$

Carbonate and silicate weathering involve fundamentally different processes. Carbonate weathering involves carbonation and congruent dissolution, whereby all products are dissolved and (through the hydrological cycle) removed from the weathering site. Silicate weathering, on the other hand, involves hydrolysis and the precipitation of secondary clay minerals; an incongruent dissolution, the products of which contribute to soil formation. Estimates of the global flux of CO_2 consumed range over 8.6–12.3 Tmol/yr (0.10–0.15 PgC/yr) for carbonate weathering, and 11.7–17.9 Tmol/yr (0.14–0.21 PgC/yr) for silicate weathering [*Meybeck*, 1987; *Gibbs et al.*, 1999; *Gaillardet et al.*, 1999; *Amiotte Suchet et al.*, 2003] (Table S1). These and other fluxes in the long-term carbon cycle are illustrated in Figure 1, with the rather conservative values used in the numerical model herein.

The chemical weathering of silicate minerals is both physically and biologically mediated. Physical erosion increases the surface area available for chemical reaction. At low erosion rates, chemical weathering can become "transport limited" by the rate of supply of new rock [*West et al.*, 2005]. At higher erosion rates there is sufficient material available such that chemical weathering becomes "kinetically limited." Then the rate of silicate weathering increases with temperature, runoff, and acidity of the weathering environment, all of which increase with the CO_2 content of the atmosphere. The resulting negative feedback is thought to be pivotal to the stabilization of the climate over Earth history [*Walker et al.*, 1981], and should also accelerate the recovery from shorter-term carbon cycle perturbations [*Lenton and Britton*, 2006]. Direct evidence for the feedback between climate and weathering comes from decades of data from Icelandic river catchments [*Gislason et al.*, 2009]. In the modern Earth system, terrestrial plants and their associated mycorrhizal fungi and soil communities also accelerate weathering rates, through increasing soil pCO_2 and carbonic acidity, secreting organic acids, physically breaking up rocks, and altering hydrology at local and regional scales [*Cochran and Berner*, 1996; *Bormann et al.*, 1998; *Kelly et al.*, 1998]. This may further alter the strength and time scale of the silicate weathering negative feedback [*Lenton and Britton*, 2006].

The time scale over which the silicate weathering feedback operates was quantified by *Sundquist* [1991]. The model used had a one-box atmosphere, coupled to a mixed layer ocean underlain by an 11-box deep ocean; each deep ocean box was coupled to a sediment box. Carbon cycle chemistry was performed using interactive variables for atmospheric CO_2, ocean dissolved inorganic carbon (DIC) and alkalinity, sedimentary $CaCO_3$, and the inclusion of simplified equations of carbonate and silicate weathering. Expressed as an *e*-folding time scale for changes in weathering rates, the silicate weathering time scale was calculated to be in the range $3–4 \times 10^5$ years. In a second study in which parameterizations of the weathering dependence on temperature and plant productivity were applied to a box model divided into atmosphere, vegetation, soil and multibox ocean, and sediments [*Lenton and Britton*, 2006], the silicate weathering time scale was determined to be of the order of

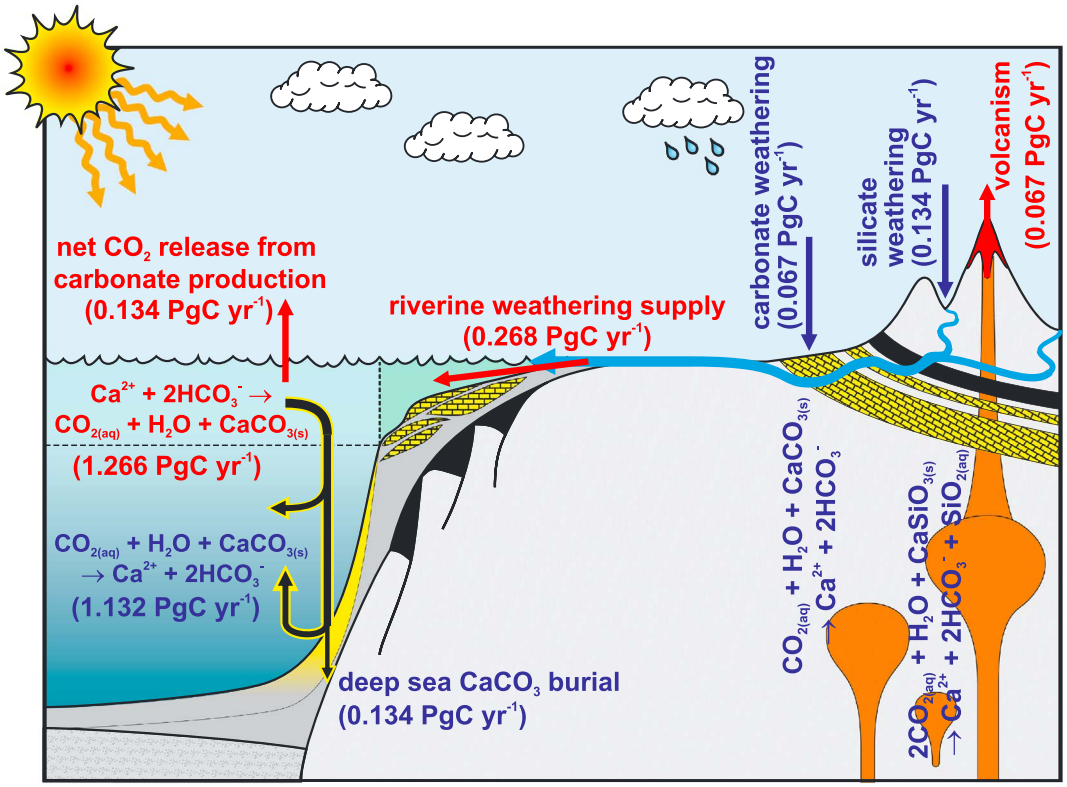

Figure 1. Illustration of the long-term (geological) carbon cycle fluxes. Shown are the long-term fluxes in the GENIE model at steady state. In red are sources of CO_2 to the atmosphere or ocean, and in dark blue are sinks of CO_2.

a million years. Other future projections of the lifetime of anthropogenic CO_2 have assumed values of 200 kyr [*Archer et al.*, 1997] and 400 kyr [*Archer*, 2005].

More recent work using spatially resolved Earth System Models (ESMs) [*Montenegro et al.*, 2007; *Ridgwell and Hargreaves*, 2007] has incorporated millennial time scale processes into modeling of the Anthropocene carbon excursion. Detailed, spatially explicit models of the carbonate sediments in the ocean are included, but terrestrial weathering processes are still only dealt with as a global average prescribed flux. As models were "only" integrated over time scales in the 10^4–10^5 year range, silicate weathering is ignored altogether; the weathering flux is from carbonates and used to quantify the effect of neutralizing fossil fuel carbonic acidity. Hence, the silicate weathering process has yet to have its time scale quantified using a spatially explicit model that includes a 3-D ocean and climate feedback on temperature and circulation.

To address this and building on earlier work, a new weathering model has been developed and incorporated into the GENIE Earth System Model [*Colbourn et al.*, 2013]. Here we use this model to quantify the time scales over which the carbonate and silicate weathering feedbacks operate under different assumptions, i.e., by including more or less processes in our model and by using different values of key parameters. The model, its parameterizations, and the ensemble members tested are outlined (in section 2 and the supporting information). Results are described with a focus on the actions of the carbonate and silicate weathering feedbacks (in section 3). Time scales analysis techniques are used to determine, from the model output, *e*-folding time scales for the reequilibration, through the action of weathering, of the Earth System, following anthropogenic carbon perturbations (section 3.2). Results are then discussed in comparison with previous work (section 4) and conclusions drawn (section 5).

2. Methods

2.1. The GENIE Model

In this work, we used *c*GENIE (mycgenie.seao2.org)—a carbon centric version of the Grid ENabled Integrated Earth system model (GENIE). GENIE belongs to the class of models known as EMICs (Earth System Models of

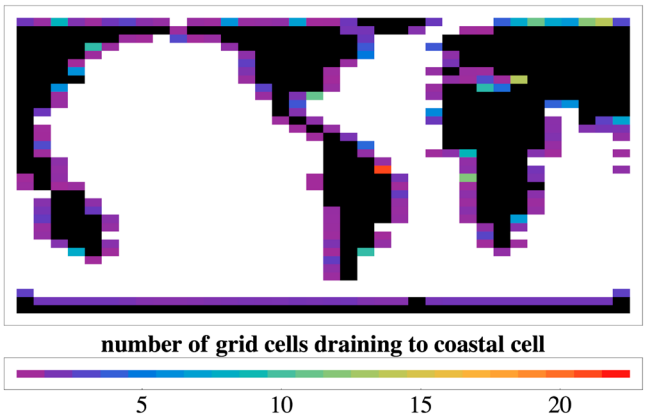

Figure 2. The GENIE model grid, showing river drainage to the coastal ocean using detailed topographical routing.

Intermediate Complexity). EMICs are often highly parameterized. Processes that take place over small spatial and temporal scales are aggregated into high-level parameterizations in order to minimize computational cost. This has the advantage of allowing more processes to be modeled and also longer integrations and larger ensembles. However, the uncertainty of model results is increased.

GENIE includes an EMBM (Energy Moisture Balance Model) 2-D atmosphere [*Weaver*, 2001] (eb), an eight-layer version of the Goldstein frictional geostrophic ocean [*Edwards and Marsh*, 2005, and references therein] (go) and sea-ice (gs); AtChem, an atmospheric chemistry module to pass gas fluxes (ac); BioGeM (BioGeochemical Model), the ocean biogeochemistry module [*Ridgwell et al.*, 2007] (bg); SedGeM (Sedimentary-Geochemical Model), the ocean sediments model [*Ridgwell and Hargreaves*, 2007] (sg); and RokGeM (Rock-Geochemical Model), the model focused on here [*Colbourn et al.*, 2013] (rg). The sediment model SedGeM calculates carbonate dissolution using the model of *Archer* [1991] explicitly, as opposed to previous work [*Ridgwell and Hargreaves*, 2007] which used a look-up table of precalculated results from the *Archer* [1991] model. The model grid is shown in Figure 2.

2.2. The RokGeM Module

The model of carbonate and silicate rock weathering, Rock-Geochemical Model (RokGeM) was incorporated in modular form into GENIE in order to explore carbon cycling over long time scales (kyr to Myr) [*Colbourn*, 2011; *Colbourn et al.*, 2013]. RokGeM calculates weathering fluxes of alkalinity and dissolved inorganic carbon (DIC) dependent on, and in feedback with, inputs of land temperature (T), runoff (R), and productivity (P). Carbonate and silicate weathering fluxes of calcium ions (F_{CaCO3} and F_{CaSiO3}, respectively) take the form

$$F_{\mathrm{CaCO_3}} = F_{\mathrm{CaCO_3},0}\left(1 + k_{\mathrm{Ca}}\left(T - T_0\right)\right)\frac{R}{R_0}\frac{P}{P_0} \tag{3}$$

$$F_{\mathrm{CaSiO_3}} = F_{\mathrm{CaSiO_3},0}e^{\frac{1000E_a}{RT_0^2}(T-T_0)}\left(\frac{R}{R_0}\right)^{\beta}\frac{P}{P_0} \tag{4}$$

where 0 denotes an initial value in the feedback ($\{T, R, P\} = \{T_0, R_0, P_0\}$ for switched off feedbacks), $k_{\mathrm{Ca}} = 0.049$ is a constant derived from correlating the temperature and bicarbonate ion concentration of groundwater [*Harmon et al.*, 1975], $E_a = 63$ kJ/mol [*Brady*, 1991] is the activation energy of the silicate weathering reaction, and β ($0 < \beta < 1$) is a fractional power dependent on lithology, with $\beta = 0.65$ [*Berner*, 1994] in the 0-D model. For this work the model was run without being coupled to a land carbon cycle model. Instead, productivity was parameterized as

$$\frac{P}{P_0} = \left(\frac{2\frac{C}{C_0}}{1 + \frac{C}{C_0}}\right)^{0.4} \tag{5}$$

following *Berner* [1991], where C is atmospheric $p\mathrm{CO}_2$.

Fluxes are worked out as a global average for the basic 0-D implementation of the model, and individually for each grid cell, for the spatially explicit 2-D version of the model—where each grid cell is apportioned between

five or six distinct lithology classes. Fluxes are routed to the coastal ocean (Figure 2) using topographic data [*Vörösmarty et al.*, 2000a, 2000b; *Colbourn et al.*, 2013], where they interact with ocean, atmosphere, and sediment biogeochemical cycles. Full details of the model are given in [*Colbourn et al.*, 2013]. Due to the coarse nature of the GENIE atmosphere model, runoff and temperature are not spatially accurate when compared to real-world data, although global averages are reasonable. Furthermore, switching between 0-D and 2-D weathering schemes when the total initial weathering flux is the same in each case, has only a tiny effect on the results that is not visible when plotting them. Hence, the 0-D (global average weathering) version of the model is focused on in this work.

To initialize the model, terrestrial weathering flux was divided evenly between carbonate and silicate weathering and set equal to a first approximation of the burial flux of carbonate material in the sediments ($F_{CaSiO_3,0} = F_{CaCO_3,0} = 5 \times 10^{12}$ mol/yr). Silicate weathering was balanced by setting volcanic outgassing equal to it. The ocean, atmosphere, and biogeochemistry were left to equilibrate under the condition of fixing atmospheric pCO_2 at a preindustrial level (278 ppm). After 25 kyr (ample time for equilibrium to be achieved), the sediments were opened and left for 100 kyr to equilibrate with the rest of the system. For this second part of the model spin-up, terrestrial weathering flux was set to equal the burial flux of carbonate as diagnosed in the first stage of the spin-up. The resulting long-term (geologic) steady state fluxes are summarized in Figure 1 (and comprise CO_2 consumption fluxes of 5.6 Tmol/yr for carbonate weathering and 11.2 Tmol/yr for silicate weathering).

2.3. CO_2 Emission Scenarios

Pulse emissions scenarios of 1000 PgC and 5000 PgC were used to model carbon cycle response over the next 1 Myr. The 1000 PgC scenario represents an approximate lower limit on cumulative anthropogenic CO_2 emissions, given historical fossil fuel emissions of 390 $\pm$ 20 PgC, historical land use change emissions of 145 $\pm$ 40 PgC, and allowing for <500 PgC future emissions. The 5000 PgC scenario has been used in previous studies [*Archer et al.*, 2009; *Montenegro et al.*, 2007] and represents a broad upper limit on conventional fossil fuel reserves/resources.

In realistic scenarios, carbon is input to the atmosphere over the course of a few hundred years. However, this time scale is a tiny fraction of the simulated time of the model runs presented here (a million years), making it of little importance for results pertaining to the far future. Therefore, as a simplification, and to aid comparison with other model studies [e.g., *Archer*, 2005; *Archer et al.*, 2009; *Cao et al.*, 2009], instantaneous pulse emissions are used in this study. In a comparison of pulse emissions with drawn out emissions, it was found that after the initial spike, the tails of the emissions curves are virtually identical [*Colbourn*, 2011].

2.4. Sensitivity Analysis

We carried out a comprehensive testing of the parameters of the RokGeM model [*Colbourn et al.*, 2013] in order to explore their effects on the uncertainty of time scales associated with weathering effects on the carbon cycle. Here we focus on the effects of switching on and off the carbonate and silicate weathering feedbacks (f_Ca and f_Si, respectively); varying climate sensitivity; varying weathering-temperature, weathering-runoff, and weathering-productivity feedbacks; the choice of river-routing scheme; and short circuiting of the atmosphere (whether carbon was removed from the atmosphere and added to the ocean or just a lower amount added to the ocean, following the stoichiometry of equations (1) and (2)). A brief description of the parameter variations considered is given in the supporting information.

2.5. Time Scale Analysis

Time scale analysis was carried out using two different methods: (1) graphing and (2) curve fitting. In the graphing method a curve was plotted of the variation with time of the difference between the reduction of each variable from its peak value, and the final reduction of each variable, taken to be at the time when the curves rate of depletion was less than 1 part in 10^6 between successive time outputs. The natural logarithm of this curve was taken, and the slope of the resulting curve was taken to be the *e*-folding time scale (i.e., for pCO_2, the time, at the given year, which it would take for the pCO_2 level to be reduced by a factor of *e*).

In the curve-fitting method, a series of exponential curves with negative gradients were fitted to model output, using the function `NonlinearModelFit` in Mathematica. The general form of the fit is given by the equation

$$V(t) = b + h \sum_{i=1}^{n} w_i e^{-(t-t_0)/\tau_i} \quad (6)$$

where V is the variable of interest, evaluated at time (year) t, b is the "baseline" of the function, or the value of the variable at the end of the decay where stabilization occurs (for ensemble members with silicate weathering feedbacks included, this is the preindustrial level), and h is the "height" of the peak above the baseline level; i.e.; the peak minus the preindustrial level. Each curve i is weighted by a normalized weighting w_i. τ_i are e-folding time scales for each curve; the time taken (t–t_0) for the curve to reach e^{-1} of its peak value, where t_0 is the time (year) of the peak. The result is a Green's function, as first used to quantify ocean CO_2 response times by *Maier-Reimer and Hasselmann* [1987].

The number of curves fitted (n), was looped over, up to a maximum of $n = 10$ (no fits had $n > 7$), in order to determine the best fitting curve. The Bayesian Information Criterion (BIC) [*Schwarz*, 1978] was used to rank curves in order of best fit, as it penalizes overfitting by giving a higher score (lower scores are best) to equal fits with more parameters.

3. Results

Here we focus on the operation of the carbonate and silicate weathering feedbacks (section 3.1), including a time scale analysis for depletion curves of key variables (excess global atmospheric pCO_2, surface warming, and surface ocean acidification) (section 3.2). The effect of climate sensitivity on weathering is also presented (section 3.3), followed by a summary of the broader sensitivity analysis (section 3.4).

3.1. Carbonate and Silicate Weathering Feedbacks

For each emissions pulse, pCO_2 initially declined relatively rapidly (over the course of a thousand years; Figure 3a). This can be attributed to "ocean invasion" of CO_2 as well as the onset of dissolution of sea bed carbonate ($CaCO_3$) sediments. The pCO_2 then declines more slowly due to the action of first carbonate and then silicate weathering feedbacks; these feedbacks include the temperature, runoff, and productivity feedbacks described in section 2.2 and discussed in detail in *Colbourn et al.* [2013].

Compared with a constant weathering flux, the carbonate weathering feedback has only a minimal effect in the long term; 50 kyr after a 5000 PgC release, there is only a 22 ppm difference in CO_2 concentrations in the atmosphere with carbonate weathering feedback switched on. Sequestration effectively stops at this point for both constant weathering (carbonate and silicate weathering feedbacks off) and carbonate weathering feedback only. The silicate weathering feedback has a more pronounced effect; a 95 ppm difference over the same 50 kyr time period. Eventually, with the action of the silicate weathering feedback, atmospheric pCO_2 is returned to near preindustrial levels, reaching 300 ppm after 440 kyr for the 5000 PgC scenario (or after 80 kyr for 1000 PgC). Interestingly, after 50 kyr, when the carbonate weathering feedback has run its course, having the carbonate weathering feedback on slightly hinders the silicate weathering feedback; in the case of both carbonate and silicate weathering feedbacks being active, it takes 460 kyr–20 kyr longer—to return to 300 ppm pCO_2 in the 5000 PgC scenario. This is likely because the carbonate weathering feedback removes CO_2 from the atmosphere, thus leaving less for the stronger silicate weathering feedback to operate on. Thus, the silicate weathering feedback is weakened in the presence of the carbonate weathering feedback.

After 1 Myr, pCO_2 is 278 and 281 ppm, respectively, for 1000 and 5000 PgC emission burns (the control run with no emissions is at 277 ppm; preindustrial pCO_2 was taken to be 278 ppm). Even on the millennial time scale, the weathering feedbacks are significant; this concurs with recent work using the UVic ESM [*Meissner et al.*, 2012]. For the 5000 PgC scenario there is a 64 ppm difference at year 3000 between having no feedbacks and having both carbonate and silicate weathering feedbacks (this represents 7% of the CO_2 in excess of the preindustrial). Other models, compared in *Archer et al.* [2009], have weathering feedback differences of 40, 50, and 135 ppm 1000 years after emissions [see *Archer et al.*, 2009, Figure 4].

Figure 3b shows the increase in atmospheric temperatures. On a millennial time scale (left panel) there is a clear lag in the system between the lowering of CO_2 levels and the lowering of temperature, illustrated by the more convex shape to the curves. The silicate weathering e-folding time scale is similar to that for CO_2 (~200 kyr); including carbonate weathering, it is slightly longer. The acidification of the oceans is illustrated in Figure 3c. Like the temperature change, the recovery of sea surface pH lags behind the reduction in atmospheric CO_2 levels.

Percentages of atmospheric pCO_2, global surface warming, and ocean acidification in excess of preindustrial levels are plotted up to year 1 M in Figure 4. The airborne fraction of excess pCO_2 (remaining) reaches 50%

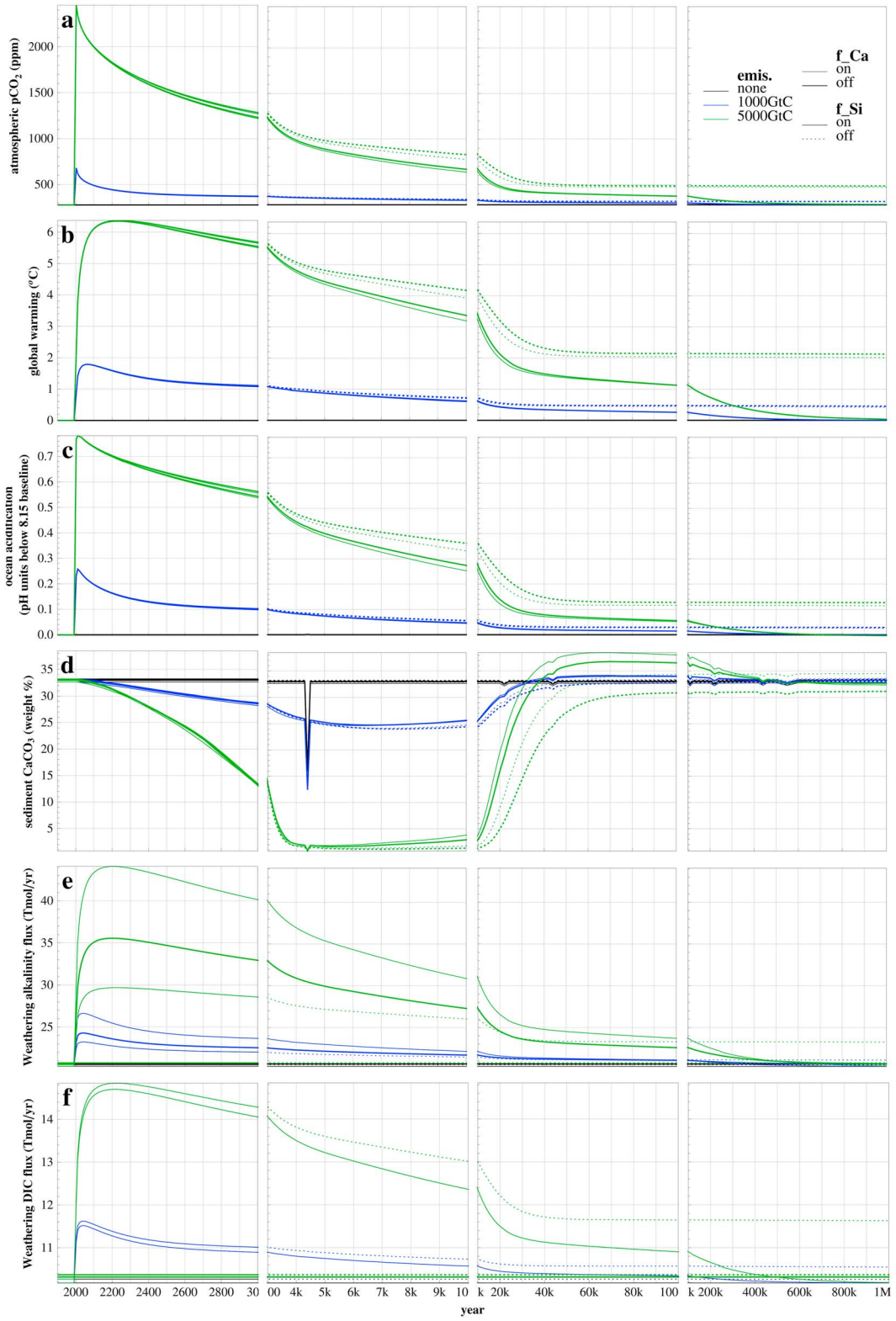

Figure 3. Evolution of (a) atmospheric pCO_2, (b) global surface warming, (c) surface ocean acidification, (d) sea floor sedimentary carbonates, (e) weathering alkalinity flux, and (f) weathering DIC flux, over 1 Myr for 1000 PgC (blue) and 5000 PgC (green) emissions pulses versus a control run with no emissions (black), with carbonate and silicate weathering feedbacks (f_Ca and f_Si, respectively) on/off in the global average (0-D) version of the model. Note that the blips in sediment $CaCO_3$ are an artifact of the model restart process (model runs were restarted every 4.4 kyr) caused by the sediments taking a few years to "warm up" and output being taken during this time.

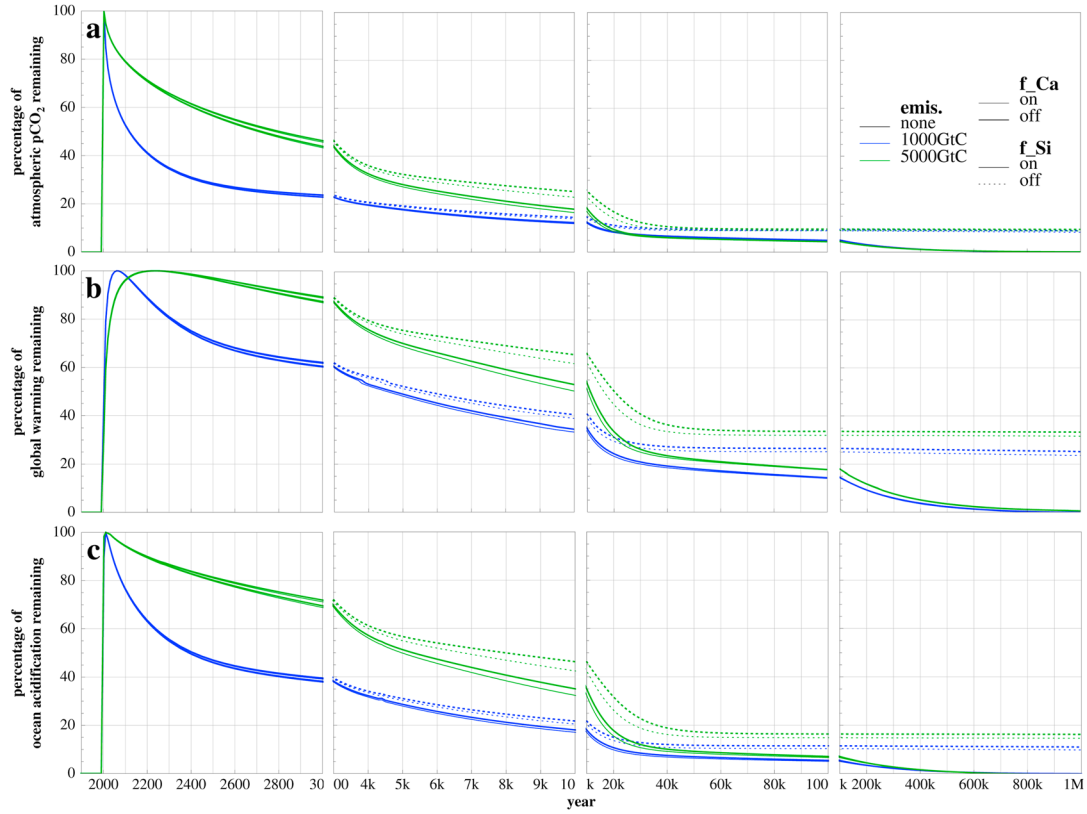

Figure 4. Fractions of initial excess atmospheric pCO_2, global warming, and ocean acidification remaining over 1 Myr for 1000 PgC (blue) and 5000 PgC (green) emissions pulses versus a control run with no emissions (black), with carbonate and silicate weathering feedbacks (f_Ca and f_Si, respectively) on/off.

by the mid-23rd century in the 1000 PgC emissions case; this milestone is not reached for a further 650 years (carbonate and silicate weathering feedbacks on) to 850 years (carbonate and silicate weathering feedbacks off) for the 5000 PgC scenario. It should be noted that due to emissions being in the form of a pulse, initial spikes in the values of the variables in question lead to an underestimation of fractions remaining when compared with more realistic scenarios, where emissions are drawn out over decades to centuries. Even so, the difference in shape between the emissions scenarios is substantial, with the larger 5000 PgC emissions leading to a steeper initial decline in fractions of excess CO_2 warming and acidification that remain. Discussing temperatures and pH values in terms of fractions (or percentages) is not strictly speaking meaningful, on account of pH being measured on a logarithmic scale and temperature depending on the logarithm of pCO_2. These variables are included in Figure 4 for the sake of allowing rough comparisons with similar figures for pCO_2 and to observe similarities and differences in the shapes and features of the curves.

The results of the graphing time scale analysis (section 2.5) are shown in Figure 5. We find a marked distinction in the response of ensemble members with fixed weathering and the carbonate weathering feedback (f_Ca), compared to those with the silicate weathering feedback (f_Si). For the atmospheric CO_2 sequestration response (Figure 5a), the fixed and f_Ca members exhibit a clear 10^4 year *e*-folding time scale between the years ~5000 and ~50,000; this is the period of "terrestrial $CaCO_3$ neutralization" through carbonate weathering [*Archer et al.*, 1998; *Ridgwell and Hargreaves*, 2007]. The exact onset and duration of this time scale is modulated by the strength of the forcing (amount of emissions); the lower forcing scenario has an earlier onset and demise of this time scale compared to the higher forcing scenario. For the f_Si runs, a ~200 kyr *e*-folding time scale emerges from year ~50,000 onward; this is the period where silicate weathering becomes dominant. After 500 kyr, the *e*-folding time scale decreases, indicating an increase in the sequestration due to silicate weathering; this is despite the approaching of preindustrial levels of carbon (see Figure 3a). This is perhaps an artifact of the analysis given the closeness of the model to reaching steady state. The peak in sequestration time scale coincides with the completion of the recovery (to preindustrial levels) of carbonate sediments in the ocean (see Figure 3d). For the carbonate weathering only runs, sequestration of

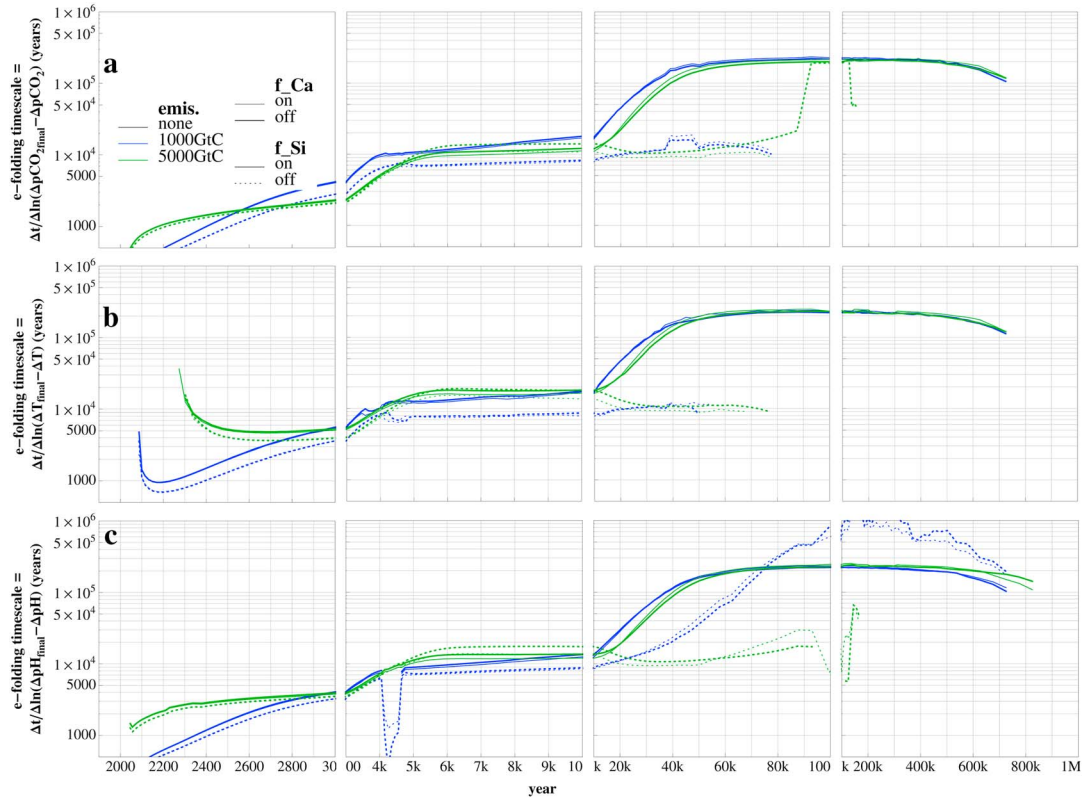

Figure 5. The *e*-folding time scales for (a) the sequestration of CO_2 from the atmosphere, (b) global surface warming, and (c) global surface ocean acidification; for 1000 PgC (blue) and 5000 PgC (green) emissions pulses versus a control run with no emissions (black), with carbonate and silicate weathering feedbacks (f_Ca and f_Si, respectively) on/off. Curves smoothed by taking a five-point moving average. Note the logarithmic scale on the *y* axis.

carbon effectively ceases after ~50 kyr (Figure 3a), giving rise to an erratic *e*-folding time scale in our analysis. Intervals between the plateaus and at the start of the simulation correspond to no single sequestration process dominating.

3.2. Extraction of pCO_2 Decay Time Scales

From the curve-fitting time scale analysis (section 2.5), for the case with both silicate and carbonate weathering feedbacks switched on, it was determined that atmospheric pCO_2 (in ppm) at year t following an instantaneous release of 1000 PgC of CO_2 emissions into the atmosphere is given by

$$pCO_2(t) = 277.6 + 308f(t) \tag{7}$$

where

$$\begin{aligned} f(t) = {} & 0.115e^{-\Delta t/25.1} + 0.36e^{-\Delta t/139} + 0.21e^{-\Delta t/350} \\ & + 0.13e^{-\Delta t/4500} + 0.09e^{-\Delta t/10200} \\ & + 0.098e^{-\Delta t/237000} \end{aligned} \tag{8}$$

is the fraction of excess pCO_2 remaining after time Δt (the time after the peak). In Table 1, the coefficients above are shown complete with errors at the 95% confidence level from the fitting. The six time scales are each likely representative of a different process in the model. Translating the *e*-folding time scales of equation (8) into half lives, what follows is a list of the time scales with the corresponding processes in parentheses: 11.5% of excess pCO_2 is removed (or "decays") with a half life of 17.4 years ("ocean invasion" and carbonate chemistry reactions in seawater); 36% has a half life of 96 years (mixing of the upper layers of the ocean); 21% has a half life of 240 years (mixing of the ocean down to depth); 13% has a half life of 3100 years (dissolution of the ocean-floor carbonate sediments); 9% has a half life of 7100 years (carbonate weathering); and 9.8% has a half life of 164,000 years (silicate weathering).

Global Biogeochemical Cycles 10.1002/2014GB005054

Table 1. Time Scale Fitting for Excess Atmospheric pCO_2, Surface Warming and Surface Ocean Acidification Decay for Model Run With the Most Realistic Parameter Set

		fit to $V(t) = b + h\sum_i w_i e^{-(t-t_0)/\tau_i}$								
Variable (V)		i	1	2	3	4	5	6	R^2	
Atmospheric pCO_2 (ppm)	b	277.6 ± 0.1	w_i (%)	11.5 ± 0.3	36 ± 1	21 ± 2	13 ± 2	9 ± 2	9.8 ± 0.1	0.99999993
	h	308 ± 30	τ_i (years)	25.1 ± 0.8	139 ± 5	350 ± 20	4500 ± 300	$10{,}200 \pm 1{,}000$	$237{,}000 \pm 3{,}000$	
Surface warming (°C)	b	-0.004 ± 0.007	w_i (%)	38.2 ± 0.4	40.4 ± 0.4	21.3 ± 0.3				0.99993
	h	1.831 ± 0.007	τ_i (years)	322 ± 9	6700 ± 200	$230{,}000 \pm 10{,}000$				
Surface ocean acidification	b	-0.0002 ± 0.0002	w_i (%)	9 ± 1	44.1 ± 0.8	9.1 ± 0.6	30.0 ± 0.5	8.25 ± 0.09		0.999993
(pH units below 8.15 baseline)	h	0.2504 ± 0.0001	τ_i (years)	47 ± 6	216 ± 8	$1{,}200 \pm 200$	7100 ± 100	$225{,}000 \pm 8{,}000$		

Note that the fractions of the perturbation attributed to the longer time scales are underestimates on account of the emissions scenario being a pulse, rather than being drawn out over decades to centuries as with our current real-world perturbation. This is because the shorter time scale processes get to remove a smaller fraction when the emissions are spread over a time scale comparable to theirs. Note also that the fractional uptake by different processes is expected to change with the size of the carbon emission pulse. In particular, the first three coefficients (0.115, 0.36, and 0.21), relating to the percentage of the carbon pulse taken up by different parts of the ocean, are expected to decline as emissions increase [*Goodwin et al.*, 2008]. These first three (submillennial) time scales are best quantified using models more complex than GENIE; GCMs with a coupled carbon cycle will give more realistic results as they have higher resolutions, dynamical atmospheres, and detailed ocean physics.

3.3. Climate Sensitivity Dependence of Weathering

A parameter affecting radiative forcing in the EMBM was adjusted so as to alter the climate sensitivity (°C of global warming for a doubling of atmospheric pCO_2). In addition to the default climate sensitivity of 2.64°C, we tested climate sensitivities of 1.5, 3, 4.5, and 6°C spanning the full range estimates as reported by the IPCC [*Solomon et al.*, 2007] (Figure S1). Time scale analysis was performed through fitting exponential curves to the atmospheric pCO_2 model output (as above). For the 5000 PgC scenario, the medium-term time scales associated with deep ocean mixing are lower for lower climate sensitivities (560 ± 6 years for 1.5°C) and higher for higher climate sensitivities (860 ± 30 years for 6°C). For higher climate sensitivities, the ocean takes longer to absorb the initial excess CO_2 on account of a decrease in ocean overturning (particularly in the Atlantic, where overturning shuts down for 2 kyr). It is worth noting, however, that the percentages of the pCO_2 perturbation sequestered over these medium-term time scales is higher for the higher climate sensitivities (55.0 ± 0.6% for 6°C versus 47.4 ± 0.1% for 1.5°C).

The situation is reversed when it comes to the long-term time scales associated with carbonate and (especially) silicate weathering. Here lower climate sensitivities give longer time scales; 9.10 ± 0.08 kyr (1.5°C) versus 6.3 ± 0.4 kyr (6°C) for carbonate weathering and 370 ± 20 kyr versus 120 ± 20 kyr for silicate weathering. Higher climate sensitivities amplify perturbations in temperature, runoff, and pCO_2, all of which in turn amplify the weathering feedbacks. These results are corroborated for the 1000 PgC scenario, which has better fits and more time scales identified [*Colbourn*, 2011].

These results suggest a way of partially determining past climate sensitivities from the paleorecord of carbon excursions; a measure of the relaxation time in carbon excursion proxies could be used to give an estimate of the climate sensitivity (assuming the perturbation size could be gauged independently).

3.4. Sensitivity Analysis

For 1000 PgC emissions, with only the weathering temperature feedback operating, the *e*-folding time scale of silicate weathering increases to ~390 kyr because of the removal of feedbacks from productivity and runoff. Then varying the activation energy of silicate weathering (E_a) over 45–103 kJ/mol gives a range of silicate weathering time scales of 420–188 kyr. With only the weathering runoff feedback operating, the *e*-folding time scale of silicate weathering increases to ~1900 kyr, indicating that variations in runoff alone can only provide a very weak long-term negative feedback on climate. Then varying the scaling factor for runoff (β) over 0.48–1.12 gives a range of time scales of 2000–890 kyr. Alternatively, parameterizing changes in runoff as proportional to changes in temperature and varying the constant of proportionality (k_run) over 0.012–0.045 yields a range of time scales of 2800–790 kyr. With only the weathering productivity feedback operating, the *e*-folding time scale of silicate weathering increases to ~710 kyr. The choice of river routing scheme used, or whether or not the atmosphere was "short circuited" in the carbon cycle, had little effect on the results.

Due to the sensitivity analysis being designed to isolate different components of the silicate weathering feedback, it does not directly yield an uncertainty range around our best estimate of the *e*-folding time scale. However, we note that individual parameter uncertainty studies produce a factor of uncertainty in the *e*-folding time scale of the silicate weathering feedback that broadly reflects the factor of uncertainty in the input parameter (e.g., variation in E_a over a factor of 2.3 yields variation in the resulting *e*-folding time scale over a factor of 2.2) and that several sensitivity studies, including varying climate sensitivity, produce a factor of 2.2–2.3 uncertainty in the silicate weathering time scale. Furthermore, the uncertainty ranges in *e*-folding time are skewed to longer time scales, with roughly two thirds of the error range above the best estimate and one third below (e.g., E_a = 74 kJ/mol gives 262 kyr, E_a = 45 kJ/mol gives 420 kyr, and E_a = 103 kJ/mol gives

188 kyr). Thus, while recognizing that this is more an expert judgment than a statistical measure, we offer an uncertainty range on the *e*-folding time scale of the silicate weathering feedback of 170–380 kyr about our best estimate of ~240 kyr from the 0-D weathering model.

4. Discussion

Fitting model output of atmospheric pCO_2 (among other variables) to a series of decaying exponentials allows us to quantify the *e*-folding time scales for various sequestration processes (see section 3.2 above). The longest time scales to come out of this analysis correspond to those of "terrestrial neutralization" through the action of carbonate weathering and, ultimately, removal of carbon to the geologic reservoir through the process of silicate weathering. Some fittings contained more time scales than others because of an overlap between the time scales of terrestrial neutralization and those of sediment dissolution. For the parameter set deemed most realistic, the carbonate weathering time scale for GENIE-RokGeM is 10.2 ± 1.0 kyr (where the error here is from 95% confidence limits in curve fitting). The sensitivity analysis suggests a more circumspect range of 8–12 kyr, dependent on the settings of various model parameters. Our estimate of the carbonate weathering *e*-folding time scale is a little longer than previous estimates of 8.2 kyr [*Archer et al.*, 1997] and 8.3 kyr [*Ridgwell and Hargreaves*, 2007].

Using our preferred 0-D global average version of RokGeM with all carbonate and silicate weathering feedbacks switched on gives a silicate weathering *e*-folding time scale of ~240 kyr, with an uncertainty range of 170–380 kyr (section 3.4).

Our estimates of the time scale of the silicate weathering negative feedback are notably shorter than the 300–400 kyr box-modeling estimates of *Sundquist* [1991]. Sundquist's study is not directly comparable, as he uses different types of perturbation and measures *e*-folding time scales for the weathering flux rather than atmospheric CO_2 (although this should make little difference). His closest perturbation is an instantaneous 10% increase in decarbonation (i.e., CO_2 input to the atmosphere) which yields an *e*-folding time scale of 380 kyr, with different experiments yielding 310 kyr and 325 kyr. The initial value of the silicate weathering flux in [*Sundquist*, 1991] is 11.8 Tmol CO_2 yr^{-1}, similar to our 0-D model, so this does not explain the discrepancy. Instead, the slower response time scale can be understood in terms of the different prescribed functional response of silicate weathering, which in *Sundquist* [1991] is

$$\frac{F_{ws}}{F_{wsi}} = \left(\frac{2R_{CO_2}}{1 + R_{CO_2}} \right)^{0.4} R_{CO_2}^{0.22} \tag{9}$$

where F_{ws} is the rate of silicate weathering; F_{wsi} the initial rate of silicate weathering, and R_{CO_2} the ratio of atmospheric CO_2 to its initial value. This contains the same productivity feedback on weathering as RokGeM, but the $R_{CO_2}^{0.22}$ term encapsulating climate feedbacks represents a weaker functional response. With our default parameter settings in RokGeM the combined temperature and runoff dependencies in equation (4) are well approximated by $R_{CO_2}^{0.4}$. Around $R_{CO_2} \sim 1$ the productivity feedback can be approximated by $R_{CO_2}^{0.2}$; thus, the total feedback about the present state is $\sim R_{CO_2}^{0.6}$ in our formulation and $\sim R_{CO_2}^{0.42}$ in *Sundquist* [1991]. If we denote the general form as $R_{CO_2}^{\alpha}$ and linearize the response about the present state (i.e., weathering flux varies as $\sim \alpha R_{CO_2}$), this suggests that the *e*-folding time scale of the silicate weathering negative feedback should scale with $1/\alpha$. We thus expect Sundquist's *e*-folding time to be ~1.4 times longer than ours based just on the weaker negative feedback—in fact it is ~1.6 times longer. The *e*-folding time scale should also scale with $1/F_{wsi}$ (the inverse of the initial weathering flux), which is similar in the two 0-D models.

The technique of autofitting a variable number of exponentials to elucidate multiple *e*-folding time scales is a useful tool for the accurate quantification of carbon cycle perturbations of any length and size. There is good potential for further work exploring the implications of this technique for quick but accurate analytical calculations of the form given by *Goodwin et al.* [2008].

5. Conclusion

We provide the first reassessment of the *e*-folding time scale of the silicate weathering feedback since *Sundquist* [1991]. A new spatially explicit weathering model, RokGeM [*Colbourn et al.*, 2013], coupled to the GENIE System Model, was used to simulate long-term carbon cycle perturbations (up to 1 Myr) in scenarios of

1000 and 5000 PgC fossil fuel emissions. The weathering time scale estimates cover a wide range depending on the parameter settings chosen. However, using the basic version of the model (global average weathering) with carbonate and silicate weathering feedbacks switched on, *e*-folding time scales of ~10 kyr (range 8–12 kyr) for carbonate weathering and ~240 kyr (range 170–380 kyr) for silicate weathering were found. The quantification of the silicate weathering time scale is the most significant result, as it has only previously been determined using box models (such as *Sundquist* [1991]) or estimated using geological evidence and reasoning [*Berner and Caldeira*, 1997]. The estimated silicate weathering time scale is shorter than in previous work, but still in the hundreds of thousands of years, suggesting a comparable duration for the Anthropocene.

Acknowledgments

We thank E. Sundquist and an anonymous referee for helpful comments. G. Colbourn acknowledges a NERC PhD Studentship, the GENIE team, and the UEA e-Science facilities. In particular, G. Williams for technical assistance with GENIE and C. Collins for helping smooth the running of hundreds of million year simulations of the Earth System. T. M. Lenton's contribution was supported by NERC (NE/G018332/2), and T. M. Lenton and A. Ridgwell were supported by the Leverhulme Trust (RPG-2013106). The *c*GENIE model code can be obtained from mycgenie.seao2.org, instructions for alternative parameter settings and data for time series output years (as plotted in Figures 3–5 and S1–S2) are given in Text S1 and Table S2 in the supporting information.

References

Amiotte Suchet, P., J. L. Probst, and W. Ludwig (2003), Worldwide distribution of continental rock lithology: Implications for the atmospheric/soil CO_2 uptake by continental weathering and alkalinity river transport to the oceans, *Global Biogeochem. Cycles*, *17*, 1038–1051, doi:10.1029/2002GB001891.

Archer, D. (1991), Modeling the calcite lysocline, *J. Geophys. Res.*, *96*, 17,037–17,050, doi:10.1029/91JC01812.

Archer, D. (2005), Fate of fossil fuel CO_2 in geologic time, *J. Geophys. Res.*, *110*, C09S05, doi:10.1029/2004JC002625.

Archer, D., H. Kheshgi, and E. Maier-Reimer (1997), Multiple timescales for neutralization of fossil fuel CO_2, *Geophys. Res. Lett.*, *24*, 405–408, doi:10.1029/97GL00168.

Archer, D., H. Kheshgi, and E. Maier-Reimer (1998), Dynamics of fossil fuel CO_2 neutralization by marine $CaCO_3$, *Global Biogeochem. Cycles*, *12*, 259–276, doi:10.1029/98GB00744.

Archer, D., M. Eby, V. Brovkin, A. Ridgwell, L. Cao, U. Mikolajewicz, K. Caldeira, K. Matsumoto, G. Munhoven, A. Montenegro, and K. Tokos (2009), Atmospheric lifetime of fossil fuel carbon dioxide, *Ann. Rev. Earth Planet. Sci.*, *37*, 117–134, doi:10.1146/annurev.earth.031208.100206.

Berner, R. A. (1991), A model for atmospheric CO_2 over Phanerozoic time, *Am. J. Sci.*, *291*, 339–376, doi:10.2475/ajs.291.4.339.

Berner, R. A. (1994), GEOCARB II: A revised model of atmospheric CO_2 over Phanerozoic time, *Am. J. Sci.*, *294*(1), 56–91, doi:10.2475/ajs.301.2.182.

Berner, R. A., and K. Caldeira (1997), The need for mass balance and feedback in the geochemical carbon cycle, *Geology*, *25*, 955–956, doi:10.1130/0091-7613.

Bormann, B. T., D. Wang, F. H. Bormann, G. Benoit, R. April, and M. C. Snyder (1998), Rapid, plant-induced weathering in an aggrading experimental ecosystem, *Biogeochemistry*, *43*, 129–155, doi:10.1023/A:1006065620344.

Brady, P. V. (1991), The effect of silicate weathering on global temperature and atmospheric CO_2, *J. Geophys. Res.*, *96*, 18,101–18,106, doi:10.1029/91JB01898.

Canadell, J., D. Pataki, R. Gifford, R. Houghton, Y. Luo, M. Raupach, P. Smith, and W. Steffen (2007), *Saturation of the Terrestrial Carbon Sink*, chap. 6, pp. 59–78, Springer, Berlin, doi:10.1007/978-3-540-32730-1_6.

Cao, L., et al. (2009), The role of ocean transport in the uptake of anthropogenic CO_2, *Biogeosciences*, *6*, 375–390, doi:10.5194/bg-6-375-2009.

Cochran, M. F., and R. A. Berner (1996), Promotion of chemical weathering by higher plants: Field observations on Hawaiian basalts, *Chem. Geol.*, *132*(1–4), 71–77, doi:10.1016/S0009-2541(96)00042-3.

Colbourn, G. (2011), Weathering effects on the carbon cycle in an Earth system model, PhD thesis, Univ. of East Anglia, Norwich, U. K. [Available at https://ueaeprints.uea.ac.uk/34242.]

Colbourn, G., A. Ridgwell, and T. Lenton (2013), The Rock Geochemical Model (RokGeM) v0.9, *Geosci. Model Dev.*, *6*, 1543–1573, doi:10.5194/gmd-6-1543-2013.

Edwards, N. R., and R. Marsh (2005), Uncertainties due to transport-parameter sensitivity in an efficient 3-D ocean-climate model, *Clim. Dyn.*, *24*, 415–433, doi:10.1007/s00382-004-0508-8.

Gaillardet, J., B. Dupré, P. Louvat, and C. J. Allégre (1999), Global silicate weathering and CO_2 consumption rates deduced from the chemistry of large rivers, *Chem. Geol.*, *159*(1–4), 3–30, doi:10.1016/S0009-2541(99)00031-5.

Gibbs, M. T., G. J. S. Bluth, P. J. Fawcett, and L. R. Kump (1999), Global chemical erosion over the last 250 My; Variations due to changes in paleogeography, paleoclimate, and paleogeology, *Am. J. Sci.*, *299*(7–9), 611–651, doi:10.2475/ajs.299.7-9.611.

Gislason, S. R., et al. (2009), Direct evidence of the feedback between climate and weathering, *Earth Planet. Sci. Lett.*, *277*(1–2), 213–222, doi:10.1016/j.epsl.2008.10.018.

Goodwin, P., and A. Ridgwell (2010), Ocean-atmosphere partitioning of anthropogenic carbon dioxide on multimillennial timescales, *Global Biogeochem. Cycles*, *24*, GB2014, doi:10.1029/2008GB003449.

Goodwin, P., M. J. Follows, and R. G. Williams (2008), Analytical relationships between atmospheric carbon dioxide, carbon emissions, and ocean processes, *Global Biogeochem. Cycles*, *22*, GB3030, doi:10.1029/2008GB003184.

Harmon, R. S., W. B. White, J. J. Drake, and J. W. Hess (1975), Regional hydrochemistry of North American carbonate terrains, *Water Resour. Res.*, *11*(6), 963–967, doi:10.1029/WR011i006p00963.

Kelly, E., O. Chadwick, and T. Hilinski (1998), The effect of plants on mineral weathering, *Biogeochemistry*, *42*, 21–53, doi:10.1023/A:1005919306687.

Le Quéré, C., et al. (2007), Saturation of the Southern Ocean CO_2 sink due to recent climate change, *Science*, *316*, 1735–1738, doi:10.1126/science.1136188.

Le Quéré, C., M. R. Raupach, J. G. Canadell, and G. Marland (2009), Trends in the sources and sinks of carbon dioxide, *Nat. Geosci.*, *2*(12), 831–836, doi:10.1038/ngeo689.

Lenton, T. M., and C. Britton (2006), Enhanced carbonate and silicate weathering accelerates recovery from fossil fuel CO_2 perturbations, *Global Biogeochem. Cycles*, *20*, B3009–3021, doi:10.1029/2005GB002678.

Maier-Reimer, E., and K. Hasselmann (1987), Transport and storage of CO_2 in the ocean—An inorganic ocean-circulation carbon cycle model, *Clim. Dyn.*, *2*(2), 63–90, doi:10.1007/BF01054491.

Meissner, K. J., B. I. McNeil, M. Eby, and E. C. Wiebe (2012), The importance of the terrestrial weathering feedback for multimillennial coral reef habitat recovery, *Global Biogeochem. Cycles*, *26*, GB3017, doi:10.1029/2011GB004098.

Meybeck, M. (1987), Global chemical weathering of surficial rocks estimated from river dissolved loads, *Am. J. Sci.*, *287*, 401–428, doi:10.2475/ajs.287.5.401.

Montenegro, A., V. Brovkin, M. Eby, D. Archer, and A. J. Weaver (2007), Long term fate of anthropogenic carbon, *Geophys. Res. Lett.*, *34*, 19,707–19,711, doi:10.1029/2007GL030905.

Revelle, R., and H. E. Suess (1957), Carbon dioxide exchange between atmosphere and ocean and the question of an increase of atmospheric CO_2 during the past decades, *Tellus*, *9*, 18–27, doi:10.1111/j.2153-3490.1957.tb01849.x.

Ridgwell, A., and J. C. Hargreaves (2007), Regulation of atmospheric CO_2 by deep-sea sediments in an Earth system model, *Global Biogeochem. Cycles*, *21*, GB2008, doi:10.1029/2006GB002764.

Ridgwell, A., J. C. Hargreaves, N. R. Edwards, J. D. Annan, T. M. Lenton, R. Marsh, A. Yool, and A. Watson (2007), Marine geochemical data assimilation in an efficient Earth System Model of global biogeochemical cycling, *Biogeosciences*, *4*, 87–104, doi:10.5194/bg-4-87-2007.

Royal Society (2009), *Geoengineering the Climate: Science, Governance and Uncertainty*, The Royal Society, London.

Schwarz, G. (1978), Estimating the dimension of a model, *Ann. Stat.*, *6*(2), 461–464.

Solomon, S., et al. (2007), Climate change 2007: The physical science basis. Contribution of working group I to the fourth assessment report of the Intergovernmental Panel on Climate Change, *Tech. Rep.*, Intergovernmental Panel on Climate Change, Cambridge, U. K.

Sundquist, E. T. (1991), Steady- and non-steady-state carbonate-silicate controls on atmospheric CO_2, *Quat. Sci. Rev.*, *10*, 283–296, doi:10.1016/0277-3791(91)90026-Q.

Vörösmarty, C. J., B. M. Fekete, M. Meybeck, and R. B. Lammers (2000a), Geomorphometric attributes of the global system of rivers at 30-minute spatial resolution, *J. Hydrol.*, *237*(1–2), 17–39, doi:10.1016/S0022-1694(00)00282-1.

Vörösmarty, C. J., B. M. Fekete, M. Meybeck, and R. B. Lammers (2000b), Global system of rivers: Its role in organizing continental land mass and defining land-to-ocean linkages, *Global Biogeochem. Cycles*, *14*, 599–622, doi:10.1029/1999GB900092.

Walker, J. C. G., P. B. Hays, and J. F. Kasting (1981), A negative feedback mechanism for the long-term stabilization of Earth's surface temperature, *Geophys. Res. Lett.*, *86*, 9776–9782, doi:10.1029/JC086iC10p09776.

Weaver, A. J. (2001), The UVic Earth system climate model: Model description, climatology, and application to past, present and future climates, *Atmos. Ocean*, *39*, 1–68, doi:10.1080/07055900.2001.9649686.

West, A. J., A. Galy, and M. Bickle (2005), Tectonic and climatic controls on silicate weathering, *Earth Planet. Sci. Lett.*, *235*, 211–228, doi:10.1016/j.epsl.2005.03.020.